Journal on Transportation System and Engineering
ISSN: 3059-9865(Print) 3059-9873(Online)
Vol. 1. Issue 2 (December) 2025: 37-49
DOI: https://doi.org/10.3126/jotse.v1i2.87742

Research Article
Received Date: May 29, 2025
Revised Date: October 9, 2025
Accepted Date: November 9, 2025
Published Date: December 21,2025

Evaluating Geogrid-Reinforced Pavements with Field-Validated Soil Models under Vehicle Load Dynamics

Aanchal Tiwari[a,*], Padma Bahadur Shahi[b] Rajan Suwal[c], Ram Chandra Tiwari[d], Prabhat Kumar Jha[e]

[a]Student, M.Sc. in Transportation Engineering, Department of Civil Engineering, Pulchowk Campus, Institute of engineering, Tribhuvan University, Lalitpur, 44700, Nepal
[b,-d]Faculty, Department of Civil Engineering, Pulchowk Campus, Institute of engineering, Tribhuvan University, Lalitpur, 44700, Nepal
[e]Engineer, Ministry of Physical Infrastructure and Transport (MoPIT), Government of Nepal

Abstract

This study investigates the application of geogrid reinforcement to improve the stress-strain behavior of pavement structures, with the goal of mitigating structural deficiencies and surface distresses. A three-dimensional numerical analysis was conducted using Plaxis software, incorporating both field and laboratory data to evaluate the suitability of various soil material models. The analysis focused on the Arughat–Okhale section of the Midhill Highway to determine the most appropriate model among the linear elastic, Mohr-Coulomb, hardening soil, soft soil, and modified Cam-Clay models. Results indicate that the linear elastic model is applicable for certain conditions, while the hardening soil and soft soil models produce outcomes that closely align with field observations. The Mohr-Coulomb, hardening soil, and soft soil models yielded similar results, whereas the modified Cam-Clay model significantly deviated from both the other models and the field measurements. These findings are based on subgrade soil modeling; applying similarly appropriate models to the other pavement layers could yield results that more accurately reflect field conditions.

Keywords: Reinforced Pavement, Soil Models, Vehicle Load Dynamics, Stress-Strain Analysis, Pavement Performance

1. Introduction

The choice of constitutive material models plays a crucial role in accurately simulating geogrid-reinforced pavement behavior under dynamic loading. Over the past decades, researchers have employed a range of models—from simple linear elastic assumptions to advanced plasticity formulations—each attempting to capture the response of flexible pavement systems. The earliest studies, such as Barksdale and Itani (1999), adopted an elastic material model to simulate pavement behavior under cyclic loading. Their work demonstrated the importance of geogrids in enhancing load-bearing capacity and minimizing deformation, setting the foundation for future numerical modeling. Al-Qadi et al. (2007) also used an elastic model to evaluate the performance of geogrid-reinforced pavements under vehicular loads. Their study highlighted the improved load distribution and reduction in surface distresses due to geogrid inclusion.

Liu et al. (2010) moved toward more realistic representations by applying the Mohr–Coulomb model for the base and subgrade layers, while maintaining a linear elastic model for the asphalt. Their findings confirmed geogrid reinforcement's effectiveness in reducing rutting and strain. Kim (2013) applied linear elastic models for asphalt and base layers, with a simplified elastic representation for the geogrid. Despite the simplicity, the study showed positive effects on deformation resistance under dynamic loading.

In 2017, two studies contributed notable insights. Ahmed Alkawaaz et al. (2017) used a 3D finite element model in ABAQUS with elastic material assumptions and validated their findings against lab tests, observing a 7.75% reduction in surface displacement. Patil and Shivananda (2017) employed PLAXIS 2D with linear elastic behavior for asphalt and Mohr–Coulomb plasticity for other layers, concluding that higher geogrid stiffness significantly reduces vertical deformation. Zhou et al. (2018) used elastic models for the asphalt layer and plastic Mohr–

Corresponding Author's Email Address 079mstre001.aanchal@pcampus.edu.np

Coulomb models for base and subgrade. Their hybrid approach revealed substantial reductions in deformation, fatigue damage, and rutting, especially in weak subgrade conditions.

Leonardi and Suraci (2022) adopted the Drucker–Prager plasticity model for unbound granular materials and incorporated a simple creep law for asphalt. This approach enabled realistic predictions of long-term deformation under repeated loads. Banerjee et al. (2022) also used PLAXIS 2D with a fully linear elastic framework to evaluate reinforced pavements. They introduced a Modulus Improvement Factor (MIF) to correlate geogrid stiffness with base layer performance and proposed a design catalogue for various traffic and subgrade conditions.

In 2023, several studies expanded on these approaches. Abdullah (2023) applied the hardening soil model for nonlinear layers like Sabkha and sand subbase, and linear elastic models for the asphalt and geogrid. The simulations were validated using wheel tracking tests and confirmed the efficacy of reinforcement. Chhetri and Deb (2023) built a 3D finite element model using linear elastic assumptions for asphalt and Mohr–Coulomb for granular and subgrade layers. Their study reported up to 49% reduction in vertical compressive strain due to geogrids. Vishwakarma and Karumanchi (2023) used a 2D axisymmetric model, combining linear elastic behavior for asphalt and Mohr–Coulomb elasto-plasticity for base and subgrade layers, showing significant rut depth reductions for low-modulus subgrades when using stiffer geogrids. Finally, Zakarka et al. (2024) advanced model fidelity by calibrating their PLAXIS 3D simulations with laboratory triaxial tests, capturing the mechanical behavior of sand reinforced with geogrids. Their study revealed increased cohesion and affirmed good agreement between numerical and experimental results.

Despite substantial research on geogrid-reinforced pavements, a key gap remains: although various studies have utilized material models such as linear elastic and Mohr–Coulomb, there has been limited systematic evaluation of their effectiveness in replicating real-world pavement behavior. Most existing work lacks direct comparison between model predictions and field-monitored or laboratory-observed responses, particularly concerning subgrade performance under dynamic loading.

This study seeks to fill that gap by focusing on the role of subgrade constitutive models in capturing pavement response under traffic loading. A full-scale geogrid-reinforced pavement section was instrumented with a GeoDynamic data logger system featuring earth pressure cells, strain gauges, and moisture sensors to monitor short- and long-term responses under the passage of a Tata 1613c truck at a controlled speed of 15 km/h. Corresponding numerical simulations were developed in PLAXIS 3D using five distinct subgrade material models—Linear Elastic, Mohr–Coulomb, Hardening Soil, Soft Soil, and Modified Cam-Clay. The Linear Elastic model assumes reversible, small-strain behavior. Mohr–Coulomb adds shear failure but lacks stiffness variation. Hardening Soil includes stress-dependent stiffness and plasticity for realistic settlements. Soft Soil targets compressible clays and organic soils. Modified Cam-Clay models critical-state behavior in normally consolidated clays. Simplicity decreases but accuracy increases from Linear Elastic to Modified Cam-Clay.

By aligning simulated outputs with field-measured stress, strain, and moisture data, this research evaluates the predictive capabilities of each model. The findings aim to inform the selection of subgrade material models in future geogrid-reinforced pavement design, ensuring closer alignment between numerical predictions and real pavement performance.

2. Study Area

The study was conducted along the Arughat–Okhale section of Nepal's Mid-Hill Road Project (Figure 1). Two pavement sections were instrumented: an unreinforced section at CH 1+700 (28°2'22.51"N, 84°48'29.03"E) and a geogrid-reinforced section at CH 1+800 (28°2'20.48"N, 84°48'27.42"E), both referenced from the bridge over the Budhigandaki River, which separates the Dhading and Gorkha districts of Nepal. Sensors including earth pressure cells, strain gauges, and moisture sensors were installed at the mid-depth of the base layer—where the 40/40Q Tensar geogrid was placed—to capture stress, strain, and moisture data under live traffic conditions (Figure 2).

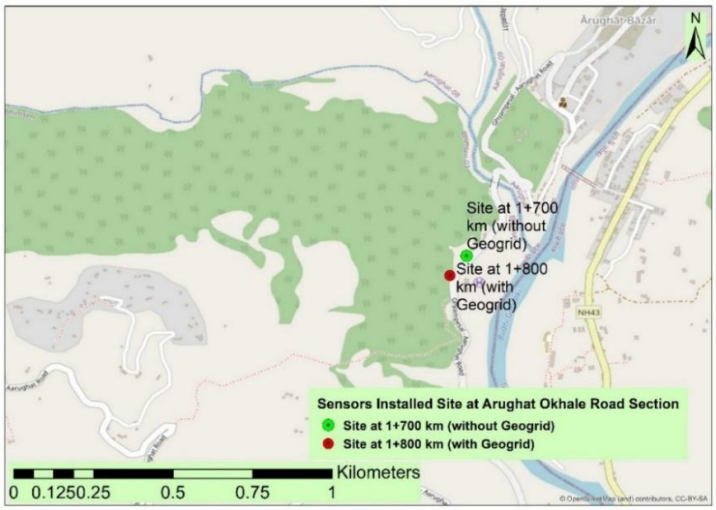

Figure 1. Study area showing test locations

Figure 2. Placement of Geogrid (40/40Q Polypropylene, bi-axial 16kN/m, Tensar Product)

3. Material and Method

This study integrates field data, lab testing, and numerical modeling to assess the performance of geogrid-reinforced pavements under real traffic conditions (Figure 3). A 3D finite element model of the Arughat–Okhale section of Nepal's Mid-Hill Highway was developed using PLAXIS 3D, reflecting the actual pavement geometry (Figure 4). Material properties were obtained through DCPT and laboratory tests (CBR, triaxial, consolidation, permeability, etc.) to define five subgrade models: Linear Elastic, Mohr–Coulomb, Hardening Soil, Soft Soil, and Modified Cam-Clay (Table 1-6).

A bi-axial polypropylene geogrid with stiffness values of 800, 1100, and 1250 kN/m was chosen for its elastic behavior to reinforce the pavement (Table 2). A point load representing the TATA TRUCK 1613C (45/55% front/rear axle distribution) was applied, and harmonic motion was generated based on vehicle speed with appropriate frequency, amplitude, and dynamic time steps. Loading conditions and wheel configurations were based on field observations, and parametric variations in geogrid stiffness and vehicle speed were included to capture realistic traffic behavior.

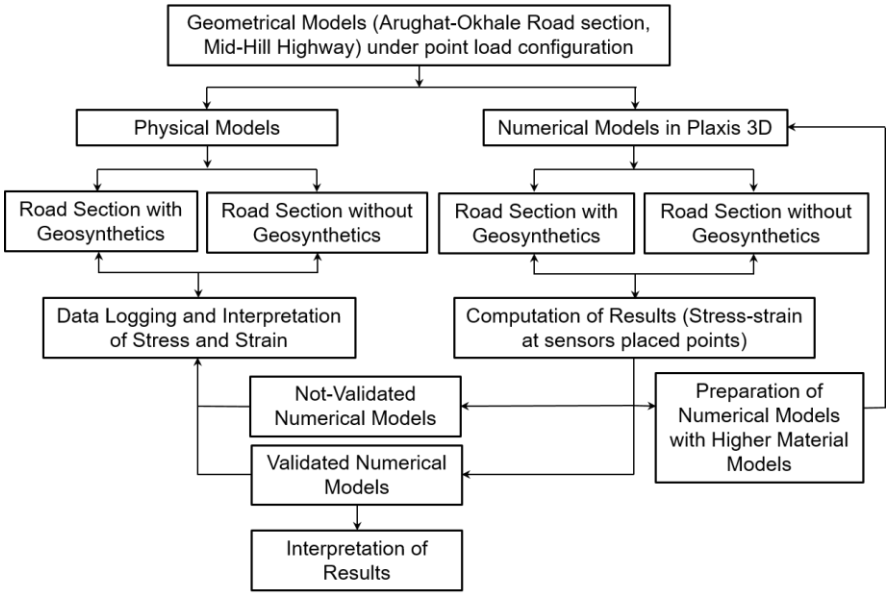

Figure 3. Methodology flow diagram

A GeoDynamic data logger system—equipped with pressure cells, strain gauges, and moisture sensors—monitored stress, strain, and moisture in the field under dynamic loading from a TATA 1613c truck at 15 km/h. Simulated pavement responses were compared against field data to determine which subgrade model most reliably reflects in-service behavior, enabling more reliable model selection for reinforced pavement design.

The numerical simulations are conducted under the same loading and boundary conditions, allowing a direct comparison between modeled outputs and measured field responses. This comparative analysis identifies which subgrade material model best represents the actual performance of geogrid-reinforced pavement, providing practical insights for improving future pavement design and reliability through better model selection.

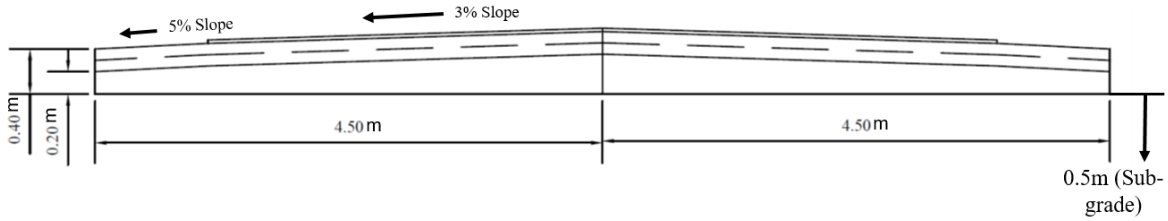

Figure 4. Geometrical model of Arught-Okhale section of MidHill Highway

Table 1. Material models for pavement structure-Linear Elastic (LE)

Item	Description
Identification	Subgrade (CBR: 5%, 5-15% for Parametric Analysis)
Material model	Linear elastic
Drainage type	Undrained-A/Drained
Unsat./Sat.unit weight, γ_{unsat} (kN/m^3)	18/20
Resilient modulus, E (MPa)	E = 10.0 * CBR for CBR ≤ 5 % & E = 17.6 * (CBR)$^{0.64}$ for CBR > 5 % (FPDG, 2014)
Poisson's ratio	0.35
Identification	Granular layer (Subbase CBR: 35%, Base CBR: 85%)
Material model	Linear elastic
Drainage type	Drained
Unsat./Sat. unit weight, γ_{unsat} (kN/m^3)	19/21

Resilient modulus, E (MPa)	$E = 0.2*(h)^{0.45} * MR_{support}$ (FPDG, 2014) Where, h = thickness in mm
Poisson's ratio	0.35
Identification	DBST
Material model	Linear elastic
Drainage type	Non porous
Unsat./Sat. unit weight, γ_{unsat} (kN/m^3)	20/-
Resilient modulus, E (MPa)	2000 (FPDG, 2014)
Poisson's ratio	0.35

Table 2. Geogrid strength properties (Bi-axial)

Item	**Description**
Identification	Geogrid Polypropylene type
Material type	Elastic
Longitudinal (EA1) & Transverse stiffness (EA2) at 2% strain (kN/m)	800 (For Parametric Analysis- 1100, 1250)

Table 3. Material models for Mohr-Coulomb (MC)

Item	**Description**
Identification	Subgrade
Material model	Mohr-Coulomb (MC)
Drainage type	Undrained-A/Drained
Unsat./Sat.unit weight, γ_{unsat} (kN/m^3)	18/20
Initial void Ratio, e_{init}	1.635
Modulus of Elasticity, E (MPa)	E = 10.0 * CBR for CBR ≤ 5 % & $E = 17.6 * (CBR)^{0.64}$ for CBR > 5 % (FPDG, 2014)
Poisson's ratio, υ	0.35
Cohesion (kPa)	9
Friction (Degrees)	28.07
Dilation Angle (Degrees), Ψ	0
Soil Type	Clay
<2µm%	10
Flow Parameter:	
Horizontal Permeability X-dir. Kx m/day	1.4655

Table 4. Material models for Hardening Soil (HS)

Item	**Description**
Identification	Subgrade
Material model	Hardening Soil (HS)
Drainage type	Undrained-A/Drained
Unsat./Sat.unit weight, γ_{unsat} (kN/m^3)	18/20
Initial void Ratio, e_{init}	1.635
Poisson's ratio, υ	0.35
Cohesion (kPa)	9
Friction (Degrees), ϕ	28.07

Dilation Angle (Degrees), Ψ	0
Secant Stiffness in Standard Drained Triaxial test $E50_{ref}$ (kPa)	18.94*e3
Tangent Stiffness for primary Odometer loading $E_{oed\ ref}$ (kPa)	15.15*e3
Loading/reloading Stiffness, E_{ref} (kPa)	$1.05*10^5$
Compression Index, Cc	0.04
Swelling Index, Cs	0.004
OCR	1.0
POP (kN/m2)	0.0
Soil Type	Clay
Horizontal Permeability X-dir. Kx m/day	1.4655

Table 5. Material models for Soft Soil (SS)

Item	**Description**
Identification	Subgrade
Material model	Soft Soil (SS)
Drainage type	Undrained-A/Drained
Unsat./Sat.unit weight, γunsat (kN/m3)	18/20
Poisson's ratio	0.35
Cohesion (kPa)	9
Friction (Degrees)	28.07
Dilation Angle (Degrees)	0
Initial void Ratio, einit	1.635
Soil Type	Clay
Horizontal Permeability X-dir. Kx m/day	1.4655
Consolidation Results:	
Tangent of the critical state, m	1.3
OCR	1.0
POP (kN/m2)	0.0

Table 6. Material models for Modified Cam-Clay (MCC)

Item	**Description**
Identification	Subgrade
Material model	Modified Cam-Clay (MCC)
Drainage type	Undrained-A/Drained
Unsat./Sat.unit weight, γunsat (kN/m3)	18/20
Initial void ratio, e0	1.635
Poisson's ratio	0.35
Cohesion (kPa)	9
Friction (Degrees)	28.07
Dilation Angle (Degrees)	0
Soil Type	Clay
Horizontal Permeability X-dir. Kx m/day	1.4655
Tangent of the critical state, m	1.3
OCR	1.0
POP (kN/m2)	0.0

Figure 5 shows the vehicle load dynamics and load configuration. Figures 6 presents the point/line load and its corresponding mesh schemes for the Tata Truck 1613c in PLAXIS 3D. Point loads simplify tire contact.

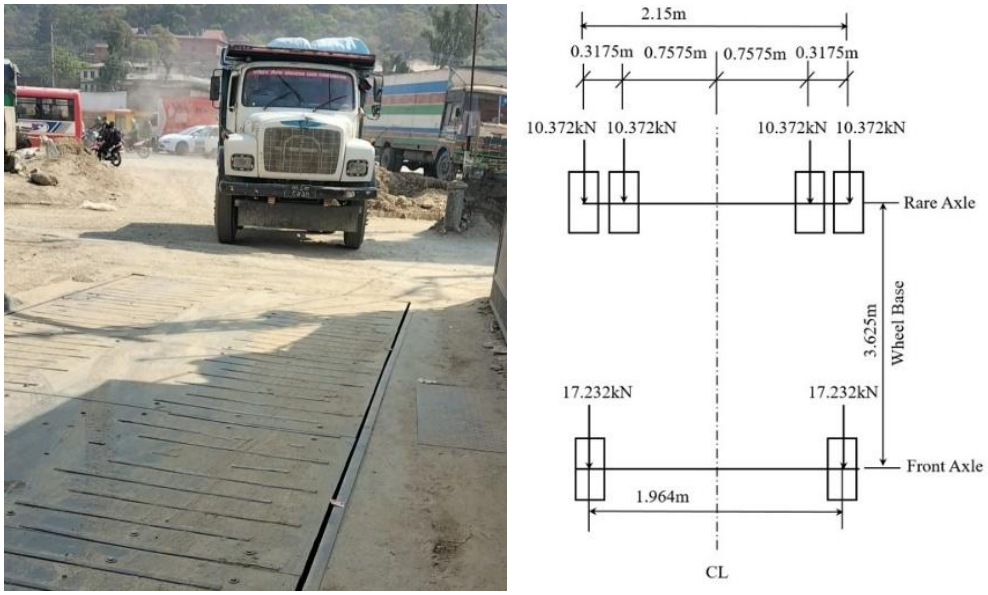

Figure 5. Vehicle load: Left Figure-Empty Truck load; Right Figure-Load configuration

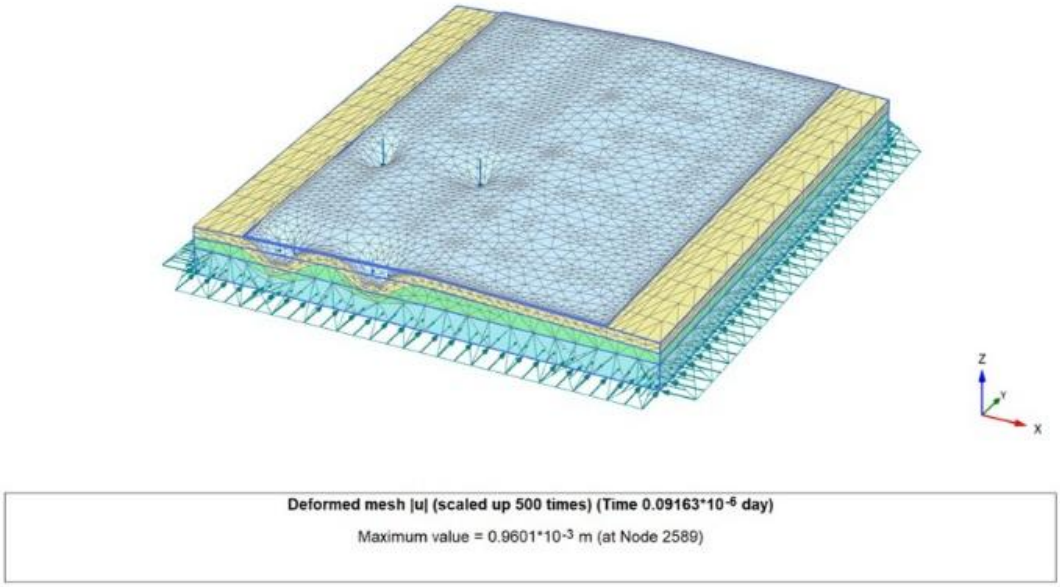

Figure 6. Meshing scheme of 6-wheels Tata Truck 1613c with Point/Line load configuration

The time cycle (Tcycle) equals the wheel perimeter divided by velocity. The motion frequency (f) is its reciprocal, and angular velocity (Ω) equals $2\pi f$. The phase angle (ϕ) is the ratio of wheelbase to curve radius, and the dynamic time step (Δt) is the time cycle divided by the number of time steps (Table 7).

Table 7. Vehicle loading condition.

Vehicle speed (km/hr)	Base frequency (Hz)	Base amplitude (m)	Accelerated amplitude at a=1.0m/sec2	Dynamic Time for time step 100 (Seconds)
15	1.25	0.531	0.584	0.00794
50	4.18	0.538	0.591	0.00171

The staged construction process in PLAXIS 3D was modeled through multiple computation phases, activating soil and structural elements as required. Dynamic analysis was carried out with deformation and mesh parameters adjusted according to geogrid activation. Vehicle movement was simulated along the Y-axis from –0.5 m to 9.5 m at speeds between 15 km/h and 50 km/h, with zero acceleration and results recorded at 100 time steps. The initial phase (K_0 procedure) established in-situ stresses, followed by plastic (static) and dynamic (moving load) phases, where displacements and strains were reset and the mesh updated. Critical nodes were monitored to assess deformation and stress–strain behavior. Static and dynamic boundary conditions assigned in the model are tabulated in Table 8.

Table 8. Static and dynamic boundary conditions assigned in the model

Boundary	BC @ X_{min}	BC @ Y_{min}	BC @ Z_{min}	BC @ X_{max}	BC @ Y_{max}	BC @ Z_{max}
Deformation	Nor. Fixed	Nor. Fixed	Fully Fixed	Nor. Fixed	Nor. Fixed	Free
Dynamic	Viscous	Viscous	None	Viscous	Viscous	None

4. Results and Discussion

4.1 Field validation

The field measurement was conducted at 15 km/hr, which is a suitable speed for capturing responses easily and reliably while observing changes during the data logging process. This measurement was mainly performed for validation purposes. Through parametric analysis, higher speed scenarios such as 50 km/hr could be simulated, representing the design speed of the Mid-Hill Highway. Simulation at this speed helps evaluate the system's response under design conditions and understand its behavior beyond the measured field condition. Data collection at different speeds could also be possible if physical modeling were carried out independently. Figures 7 to 10 illustrate the comparison between numerical simulation and field measurements for geogrid-reinforced pavement under a Tata Truck 1613c moving at 15 km/h. Figures 7 and 9 show simulated principal stress and total displacement across the pavement width, while Figures 8 and 10 present corresponding field data from earth pressure cells and strain gauges. This comparison helps validate the numerical model's ability to capture real pavement behavior under dynamic loading. In Figure 7, the left figure shows a sectional view of the Principal stress 'Sigma 1' along the pavement's symmetric half-width, while the right figure compares the static and dynamic cases. The dynamic case shows higher stress values, with a maximum of -6.095 kN/m² and a minimum of -16.24 kN/m². Figure 8 displays field measurements confirming these results, with fluctuations observed in the pavement width as mentioned in Figure 7.

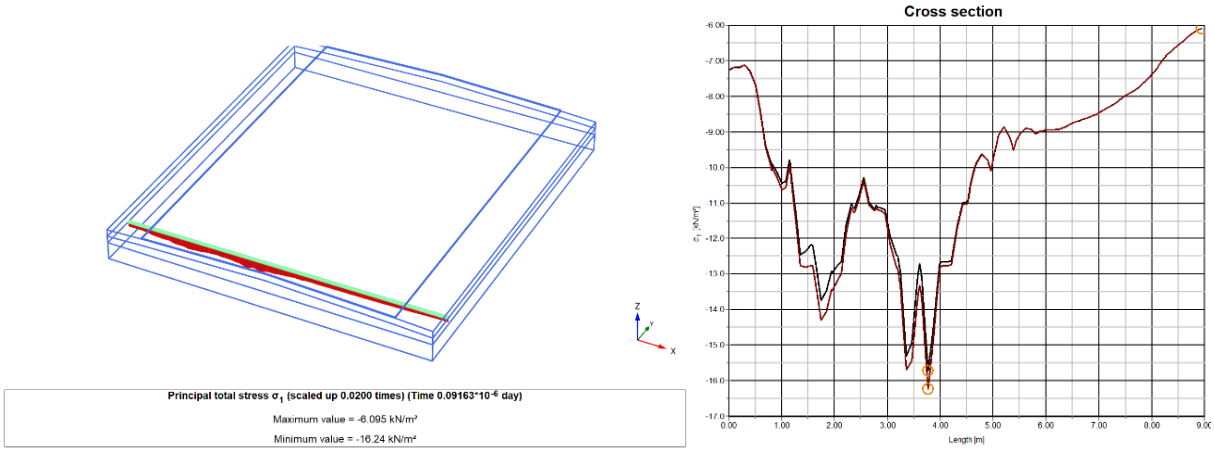

Figure 7. Principal stress (σ_1 in kN/m²) along the symmetric half-width of the pavement (transverse direction) at a constant speed of 15 km/h. Left: Stress distribution at Section 1; Right: Sectional view of stress profile.

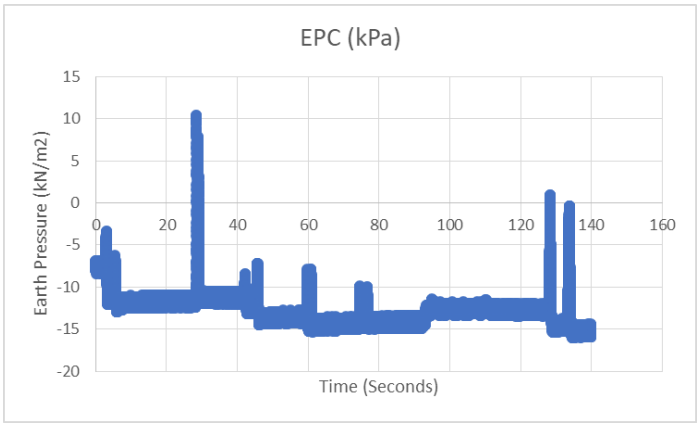

Figure 8. Earth Pressure–Tata Truck 1613c at 15 km/h, Matching Figure 8

Figure 9 shows the computational results for the pavement model with Tata Truck 1613c under a point load, reinforced with geotextile at a speed of 15 km/h. The left figure presents a sectional view-1 of the total displacement 'u' along the symmetric half-width of the pavement, while the right figure compares the static and dynamic cases. The maximum total displacement value obtained is 0.09940×10^{-3} m. Figure 10 shows that field observation confirms the numerical evaluation presented in Figure 9. The deformation pattern indicates that geotextile reinforcement effectively reduces surface displacement and distributes load stresses more uniformly. The close agreement between field and numerical results validates the reliability of the adopted material model and analysis approach.

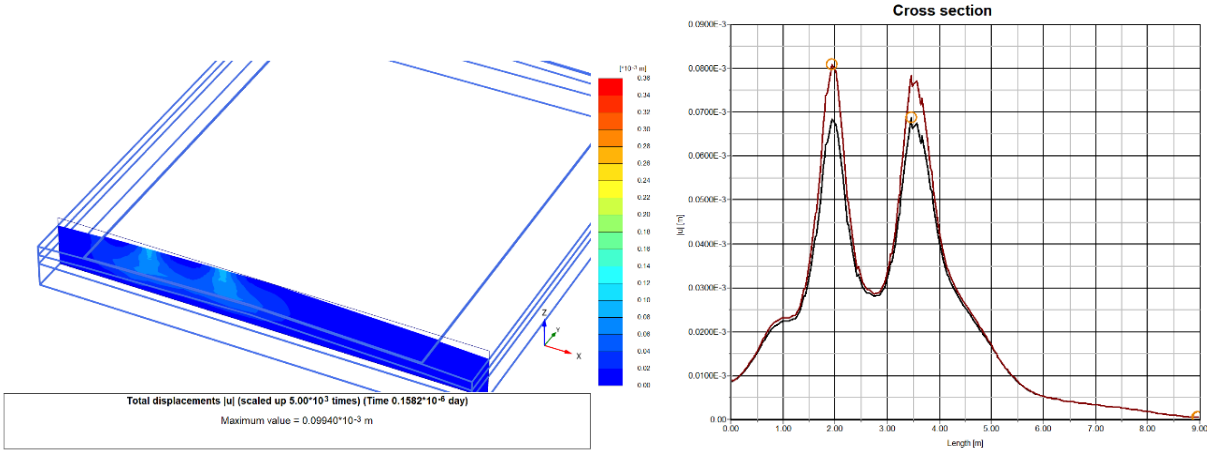

Figure 9. Total displacements (u in m) along the symmetric half-width of the pavement (transverse direction) at a constant speed of 15 km/h. Left: Displacement at Section 1; Right: Sectional view of displacement profile

Figure 11 (Left) shows the stress at the mid-base under a point load from a Tata Truck 1613c at 15 km/h and 1.0 m/s² acceleration, with stress reductions ranging from 6.66% to 40.15% due to geogrid reinforcement. Figure 11 (Right) displays the stress at 50 km/h and 1.0 m/s² acceleration, where geogrid reinforcement results in a reduction of 6.91% to 21.85%.

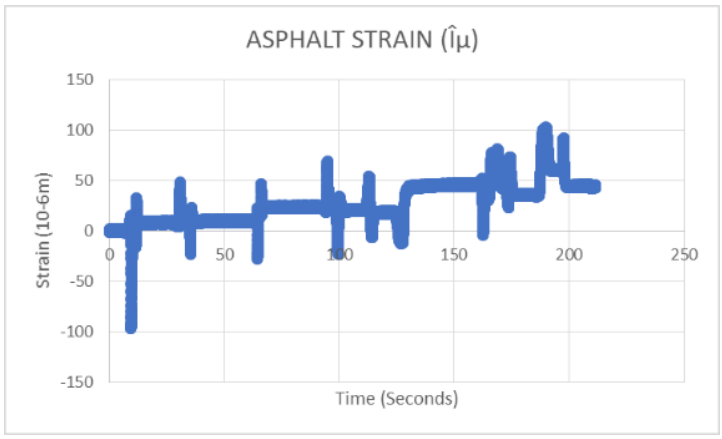

Figure 10. Strain Gauge data–Tata Truck 1613c at 15 km/h, Matching Figure 10

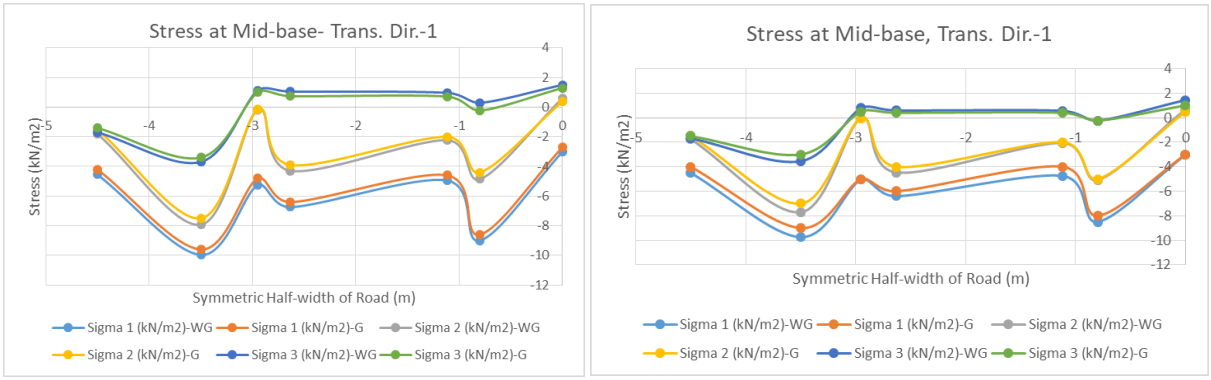

Figure 11. Mid-base stress at 1.0 m/s² acceleration (Tata Truck 1613c), Transverse-1: Left Figure - 15 km/h; Right Figure- 50 km/h, geogrid (G)/without geogrid (WG).

Figures 12 left and right show the variation of principal stress (σ_1) in both transverse and longitudinal directions for cases without and with geogrid reinforcement, respectively. In the absence of geogrid, the stress at higher speeds is observed to be lower. However, in the geogrid-reinforced case, the stress values exhibit both higher and lower extremes. This variation may be attributed to the membrane effect of the geogrid, which influences the stress distribution within the pavement structure.

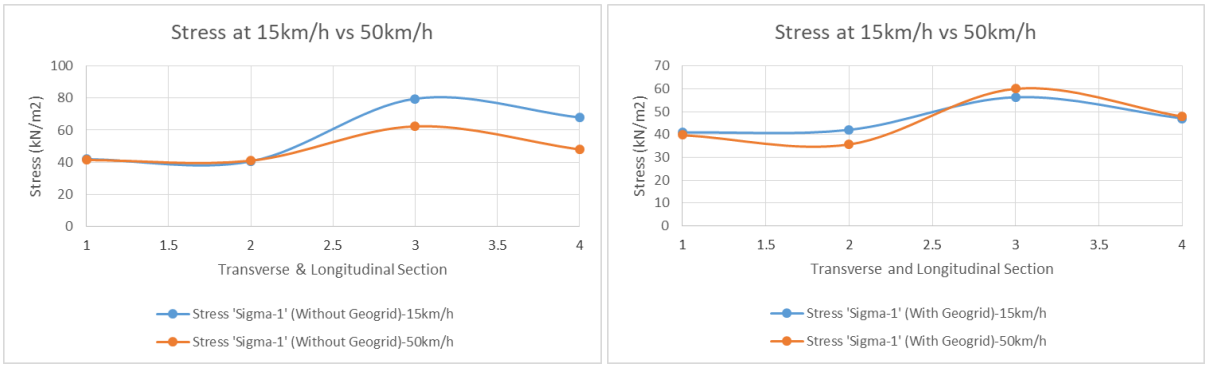

Figure 12. σ_1 Variation (Transverse & Longitudinal): Left Figure-without Geogrid (WG); Right Figure-with Geogrid (G)

4.2 Modeling with Higher Material Models

This modeling is conducted specifically for the subgrade soil layers, while the remaining pavement layers are kept consistent across all cases. Field data were recorded at a speed of 15 km/h for the TATA Truck 1613c, and the analysis further explores potential variations at higher speeds. The Table 9 presents the principal stress (σ_1 in kN/m²) and total displacement (u in meters) obtained from various material models: Linear Elastic, Mohr-Coulomb, Hardening Soil, Soft Soil, and Modified Cam-Clay.

The material models aligned with field measurements were identified using data from the TATA Truck 1613c moving at a constant speed of 15 km/h. Two criteria were evaluated: stress and deformation. Under the stress criterion, all material models—except the modified Cam-Clay model—produced results closely matching field observations. The percentage differences in stress compared to field data are as follows: Linear Elastic – 10%, Mohr-Coulomb – 6.93%, Hardening Soil – 12.3%, Soft Soil – 0.91%, and Cam-Clay – 18.51%. Among these, the Soft Soil model showed the best agreement with field data, although the Linear Elastic, Mohr-Coulomb, and Hardening Soil models are also reasonably applicable. Considering the deformation criterion, the Hardening Soil model shows the closest agreement with field measurements, with a difference of just 1.08%. In comparison, the differences for other models are: Linear Elastic – 27%, Mohr-Coulomb – 43.67%, Soft Soil – 16.27%, and Cam-Clay – 187%. However, all models except the Cam-Clay model are reasonably applicable to field conditions. In summary, the Linear Elastic, Mohr-Coulomb, Hardening Soil, and Soft Soil models can be used with confidence. Among them, the Hardening Soil and Soft Soil models show the best alignment with field data based on both stress and deformation criteria.

Table 9. Material Model(s) aligned with Field Measurements

Field Measurement vs Numerical	Field Measurement	Linear Elastic	Mohr-Coulomb	Hardening Soil	Soft Soil	Modified Cam-Clay
Stress (kN/m2), % difference	30.00	33.00 (10%)	32.08 (6.93%)	33.70 (12.3%)	**29.73 (0.9%)**	24.45 (18.5%)
Displacement (mm), % difference.	1.29	0.93032 (7.88%)	0.7266 (43.67%)	**1.276 (1.08%)**	1.08 (16.27%)	3.705 (187%)

The stress distribution at the mid-base under point loads from the Tata Truck 1613c was analyzed for various road directions (transverse and longitudinal) at a speed of 50 km/h and an acceleration of 1.0 m/s², with and without geogrid reinforcement. Without geogrid, significant stress concentrations were observed, especially in the transverse direction and longitudinal direction-2. When geogrid was applied, stress levels were significantly reduced, particularly in the transverse directions, indicating better load distribution and reduced stress concentrations, enhancing durability under heavy load conditions (Figure 15 and 16). In Figure 13 (left), stress at the mid-base in the transverse direction-1 without geogrid shows significant increases in stress compared to the Linear Elastic (LE) model, with Mohr-Coulomb (MC) at 105.57%, Hardening Soil (HC) at 150.40%, Soft Soil (SS) at 143.46%, and Modified Cam-Clay (MCC) at 268.86%. The HC and SS models show similar stress values, closer to the MC model, while the MCC model deviates significantly. In Figure 13 (right), stress in the longitudinal direction-2 shows similar behavior across all material models, with no significant change in stress percentage, although all models differ from the LE model. In Figure 13, Longitudinal-2 refers to the second wheel position along the wheel path of the TATA truck, taken at 9.5 m. Transverse-2 refers to the rear wheel position along the wheelbase side, taken at 3.5 m, representing the symmetric half of the model according to the vehicle load configuration and dynamics.

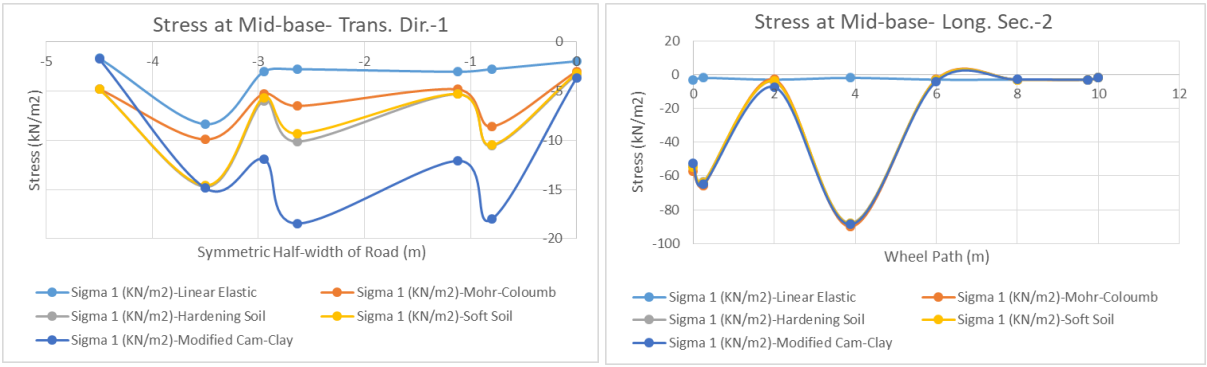

Figure 13. σ_1 stress at Mid–base (Truck, 50 km/h, 1.0 m/s²): Longitudinal–2, without Geogrid; Right–Transverse-2, with Geogrid

Figure 14 (left) illustrates the stress (Sigma 1) at the mid-base under a point load from a Tata Truck 1613c in the transverse direction-2, with geogrid reinforcement, at 50 km/h and 1.0 m/s². Stress reductions compared to the Linear Elastic (LE) model are: Mohr-Coulomb (MC) 0.64%, Hardening Soil (HS) 4.26%, Soft Soil (SS) 1.86%, and Modified Cam-Clay (MCC) 60.19%, with MCC showing the largest deviation. Figure 14 (right) shows stress (Sigma 2) in the longitudinal direction-2, with geogrid reinforcement, where the percentage changes are: MC 2.73%, HS 13.75%, SS 11.04%, and MCC 18.15%. The MC method is closest to the LE model, while HS, SS, and MCC show similar results to each other.

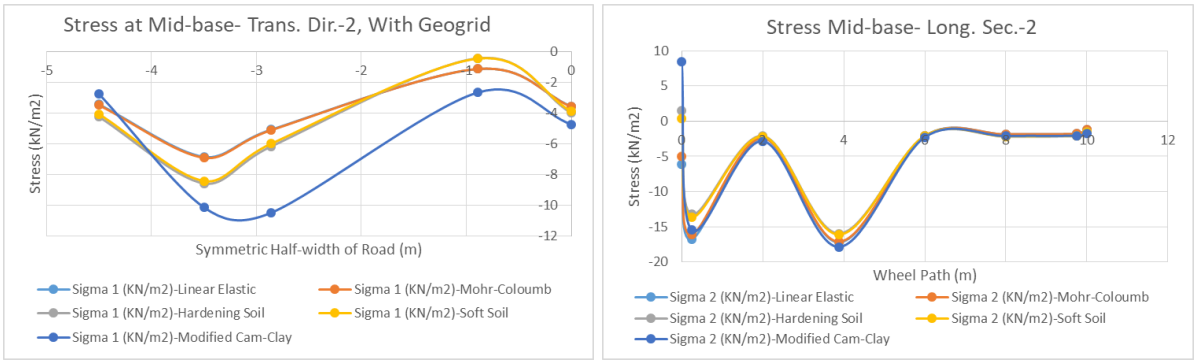

Figure 14. σ_2 Stress at Mid–base (Truck, 50 km/h, 1.0 m/s²): Longitudinal–2, with Geogrid; Transverse–1, without Geogrid

5. Conclusion and Recommendations

This study assessed the effectiveness of geogrid by validating various subgrade material models against field-monitored stress and deformation. Among the five constitutive models tested, significant variation in predictive accuracy was observed. The Soft Soil and Hardening Soil models showed strong alignment with field results, while simpler models like Linear Elastic offered reasonable performance for general use. Key findings are as follows:

- SS model: Best for stress prediction (0.91% deviation); closely matched field data.
- HS model: Most accurate for deformation (1.08% deviation); effectively captured subgrade behavior.
- LE model: Simple and efficient; moderate accuracy (10% stress, 27% deformation deviation).
- MC & MCC models: Moderate to poor alignment; MCC showed the highest deviation and is least suitable.

The study ensures model reliability by aligning numerical results with field measurements and performing parametric analyses across different geogrid stiffnesses and vehicle speeds, effectively capturing real-world traffic behavior and supporting the robustness of the results.

Acknowledgments

We would like to express our gratitude to QRDC, the DOR, and RTU, Pulchowk Campus, for their funding and support in instrumentation. Special thanks to Er. Hemant Tiwari, SOTEN, for his continuous encouragement.

References

Abdullah, G. M. S. (2023). Performance of Enhanced Problematic Soils in Roads Pavement Structure: Numerical Simulation and Laboratory Study. Sustainability, 15(3), 2595. https://doi.org/10.3390/su15032595

Ahmed Alkawaaz, N. G., AL-Badran, Y. M., & Muttashar, Y. H. (2017). Evaluation of Geogrid-Reinforced Flexible Pavement System Based on Soft Subgrade Soils Under Cyclic Loading. Al-Mustansiriyah University.

Al-Qadi, I. L., Ozer, H., & Elseifi, M. A. (2007). Evaluation of geogrid-reinforced pavements. *Journal of Geotechnical and Geoenvironmental Engineering*, 133(12), 1537-1547.

Banerjee, S., Srivastava, M. V. K., Manna, B., & Shahu, J. T. (2022). A Novel Approach to the Design of Geogrid-Reinforced Flexible Pavements. Int. J. of Geosynthetics and Ground Engineering, 8:29. https://doi.org/10.1007/s40891-022-00373-3

Barksdale, R. D., & Itani, R. H. (1999). Design and construction of pavement geosynthetics. *Transportation Research Record*, 1638(1), 37-43.

Chhetri, S., & Deb, P. (2023). Finite Element Analysis of Geogrid-Incorporated Flexible Pavement with Soft Subgrade. Appl. Sci. 2024, 14(13), 5798. https://doi.org/10.3390/app14135798

Federal Highway Administration (FHWA). (2014). Flexible pavement design guide (FPDG).

Kim, Y. (2013). Effectiveness of geogrid reinforcement in flexible pavements under dynamic loading. *Geotextiles and Geomembranes*, 41(2), 77-84.

Leonardi, G., & Suraci, F. (2022). A 3D-FE Model for the Rutting Prediction in Geogrid Reinforced Flexible Pavements. Sustainability, 14(6), 3695. https://doi.org/10.3390/su14063695

Liu, W., Zeng, H., & Chen, G. (2010). Impact of geogrid reinforcement on the performance of flexible pavements. *Geotextiles and Geomembranes*, 28(3), 261-268.

Patil, C. C., & Shivananda, P. (2017). Effect of Axial Stiffness of Geogrid in the Flexible Pavement Deformation through Finite Element Analysis with PLAXIS 2D. JETIR, 4(11), 375–381.

Vishwakarma, P., & Karumanchi, S. R. (2023). Modeling of Semi-Mechanistic Approach for Geo-synthetic Reinforced Flexible Pavement Design. Proceedings of the 9th International Congress on Environmental Geotechnics (9ICEG), Chania, Greece.

Zakarka, M., Skuodis, Š., & Kuhlmann, J. (2024). Geogrid reinforced soil model calibration based on laboratory testing. In Proceedings of the 28th European Young Geotechnical Engineers Conference (EYGEC 2024). Macedonian Association for Geotechnics.

Zhou, Z., Zhang, L., & He, L. (2018). Improvement of pavement performance with geogrid reinforcement: A laboratory and numerical study. *Soil Mechanics and Foundation Engineering*, 55(1), 52-60.